Exploiting Mallows Distance to Quantify EEG Distribution for Personal Identification

Baicheng Chen[1], Kun Woo Cho[2], Chenhan Xu[1], Feng Lin[3], Zhanpeng Jin[1] and Wenyao Xu[1]
[1] University at Buffalo, the State University of New York, Buffalo, New York, USA
[2] Princeton University, Princeton, New Jersey, USA
[3] Zhejiang University, Hangzhou, Zhejiang, China

***Abstract*—Electroencephalogram (EEG) activity from the brain is a promising biological marker that can serve as personal identification. Despite substantial efforts, it still remains unsolved problems to quantify EEG feature distribution for brain biometrics due to the complexity of the brain. In this study, we attempt to tackle EEG-based identification challenges by exploiting a novel distribution model. The distribution dissimilarity is measured by Mallows distance, a cluster similarity sensitive distance that is robust to signal noises. Specifically, EEG signals are decomposed through several statistical feature extraction methods, autoregressive (AR) model, discrete wavelet transform (DWT), and fast Fourier transform (FFT). With the dataset obtained from the real-world application, our proposed system achieves the f-score accuracy of 96.18% and half total error rate of 2.223%, which demonstrates the feasibility and effectiveness of utilizing EEG biometrics for personal identification applications.**

***Index Terms*—Biometrics; Secure Authentication; Wearable Computing**

I. Introduction

Biometrics has been developed for decades as a personal identification mechanism to secure information [19], [37] by verifying the user's identity before granting access, anthropocentric traits are now playing pivotal roles in everyday user authentication for both privacy and security purposes. Their applications cover a wide variety of scenarios, from authenticating a user through fingerprint, face or iris, banking service authentication using voice, medical analysis using gait, to governmental agency utilizing DNA toward citizen identification [3], [6], [32]. Moreover, innovative biometric modalities, including palm vessel [24], heartbeat [26], and pulse [30], are recently investigated and indicate promising performance. The advancement of biometrics provides tremendous security and safety benefits to civilians.

Among existing anatomical and behavioral biometrics, the EEG signal is one of the metrics related to individual-specific human characteristics and has been newly emerged as a resource for biometrics-based personal identification. The human brain is highly complex and dynamic as it operates information at high speed and quantity. This results with EEG signals acquired from the brain also being highly complex and dynamic. The complexity of comprehension adds a level of security in terms of being less prone to spoofing and counterfeiting attacks. Compare to other biometric techniques such as DNA testing and gait analysis, the recording of EEG signals is non-invasive and non-dispersal, which significantly reduces user discomfort as well as prevents an attacker from EEG response pilfering.

Therefore, it is highly feasible to replace currently existing biometric identification methods based on DNA, fingerprint, voice, gait, and iris [31] with EEG in personal identification applications.

A. Related Work

Most of the prior works related to EEG-based identification have mainly focused on the classification of pathologically induced EEG signals, which has abnormalities due to serious psychiatric disorders, such as epilepsy or schizophrenia [16], [21]. However, the success in distinguishing pathological EEG signals from a healthy subject using particular signal analysis methods like discrete wavelet transform and fast Fourier transform demonstrates that specific variations in the EEG pattern can serve as a good resource for a non-clinical personal identification [16], [29], [36].

The concept of using healthy EEG signal for personal identification has been validated by several studies in the past. For instance, Poulos $et\ al.$ presented the person identification using EEG of healthy individuals by implementing a set of non-linear model parameters as a feature of EEG signal. This model was then classified by an artificial neural network classifier. Although the classification accuracy of the method was not high enough ($76-88\%$ for accuracy) for a direct implementation of EEG identification, their results prove that the EEG can be successfully exploited for subject identification [31]. Similarly, Mohammadi $et\ al.$ proposed a personal identification using the autoregressive model for EEG signals and achieved the classification score in the range of $80-100\%$ [28]. Gui $et\ al.$ studied a set of event-related potential patterns to identify users [12]–[14]. Recently, Lin $et\ al.$ applied brain biometrics in wearable and mobile applications for secure user authentication [25].

B. This Work

In our work, we present a new EEG feature distribution distance computation mechanism for personal identification by adopting Mallows Distance. One of the biggest problems of EEG biometrics is the very small signal-to-noise ratio (SNR) of the signals coupled by a variety of noise sources [34]. To address this problem with noises in EEG, our work utilizes EEG signal as a feature distribution and computing the dissimilarity

978-1-7281-2319-6/19/$31.00 ©2019 IEEE

measure of EEG distributions with Mallows distance [27]. To the best of our knowledge, our work is the first paper to utilize Mallows Distance for EEG identification system. Since Mallows distance matches distributions in two clusterings in a globally optimal manner and is known to be robust to signal noises, utilizing Mallows distance allows the matching of the signal distributions in a very natural way, therefore provides better performance than other measures [35], [39].

We summarize our contribution to three-fold:

- We investigate the feasibility of EEG biometric identification utilizing Mallows distance in feature distribution's dissimilarity measure.
- We implement Mallows distance based EEG identification system with a machine learning algorithm to verify the feasibility of a person identification system with Mallows distance.
- We evaluate the performance of implemented identification system to demonstrate the capabilities of a person identification system utilizing Mallows distance.

This paper is structured as follow: Section II provides the details of data acquisition and EEG recording procedures. Section III describes the development of our EEG-based personal identification system, which is subdivided into the feature extractions, Mallows distance, and the classification with SVM. Then, Section IV provides a description and discussion of the performance evaluation. Lastly, Section V concludes the paper.

II. Materials

We utilize the publicly available database provided by the Swartz Center for Computational Neuroscience Foundation (SCCN) to perform EEG-based personal identification via Mallows distance [10]. The data is organized with respect to participant number, target stimuli type, and a series of stimuli. Using Neuroscan software, the collection of multiple channel data are acquired from 10 healthy subjects (6 males, 4 females). Also, this public database has been pre-processed through Neuroscan software to remove any idiosyncrasies that resulted from the recording set-up.

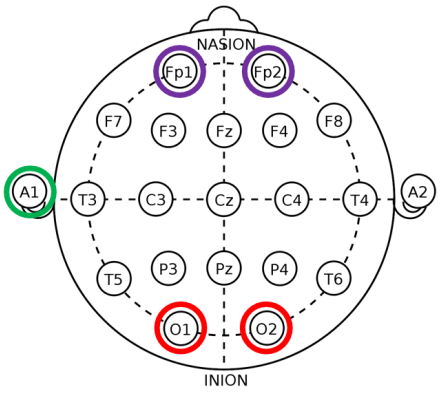

Fig. 1. Standard electrode location.

A. Channel Selection

According to Altahat *et al*. [2], O2 has the highest channel stability value among 64 channels. Such stability will allow high consistency in terms of repeating signal characteristics over a long period, this is highly preferred. Also, the channel stability of O1 ranked fourth out of 64 channels. These results demonstrate that O1 and O2 are highly recommended EEG channels to be used in biometrics as an alternative to the complete EEG channel set. The position of O1 and O2 is very close to the visual cortex of the brain structure which is responsible for visual input processing, this provides insight to the use of O1 and O2 along with EEG response from the target and non-target stimuli. Examples of target stimuli and non-target stimuli are shown in Fig. 2, each target stimuli have a distinguishable target object in the image, and each non-target stimuli image lack a main target for focus. Instead of using all-electric brain potentials recorded from 64 electrodes, we selected O1 and O2 (International 10-20 System) electrodes for better computational efficiency and stability over time of our identification system. Moreover, electrode A1 is used as a reference, and Fp1 and Fp2 electrodes are used as grounds (See Fig. 1). The data acquisition was made at a sampling rate of 1000 Hz, which corresponds to a sample bin of 1 ms, and the impedance was kept below 5 kOhms. This recording is processed through a SynAmps system coupled with a personal computer [9].

B. Experimental Details

In this section, we provide a detailed description of experimental procedure for EEG signal acquisition from participants that contributes toward personal authentication. Each participant performs a categorization task of photographs. In the task, target and non-target images were equally likely presented. There were 4 series with 100 images per each series. During each series, participants were instructed to press a touch-sensitive button, and as the eight-bit color photograph flashes, they were told to show their responses following the go and no-go paradigm. When the target image flashes, they lifted their finger from the button within 1 000 ms, and any delay is considered as a no-go response. The image was flashed for only 20 ms to avoid the use of exploratory eye movement. If the image is not a target picture, participants continued pressing the button at least 1000 ms. The stimulus onset asynchrony was 2000 ms. As mentioned above, each task was organized in a series of 100 images, which are composed of 50 target stimuli mixed with 50 non-target stimuli. The target stimuli included the pictures of animal, such as mammals, birds, fishes, arthropods, and reptiles while the non-target stimuli depicted the natural landscapes or city scenes, pictures of food, fruits, vegetables, and trees [9]. Our study aims to investigate the EEG pattern of individuals responding to the target visual stimulus. Thus, our system selectively employs target pictures as visual stimuli set and then provide a comparison against non-target visual stimuli in evaluation.

(a) Example of Target Stimuli

(b) Example of Non-Target Stimuli.

Fig. 2. Example of stimuli used toward EEG signal acquisition.

III. Methods

The overall identification process of our system is shown in Fig. 3. To illustrate our implemented system, we utilize this section to provide details of our feature extraction methods, distance computation algorithm, and the classification of calculated distances using a linear support vector machine.

First, we present our Identification Algorithm Illustration to modulize our methodology:

- **EEG Signal Acquisition:** Signal $\rho(t)$ is collected in the temporal domain with t being time.
- **Signal Feature Extraction:** Feature set $\phi(n)$ is extracted from $\rho(t)$ with n being total number of features.
- **Mallow Distance Calculation:** Mallow distance M is calculated based on the feature set $\phi(n)$.
- **SVM Classification:** Prediction result C from SVM model is generated using mallow distance M with C.

A. Feature Extraction

To capture the unique characteristics of each EEG signal as well as to reduce the dimension of data, we extract feature values from the EEG signal to perform classification.

As shown in Table II, five statistical features are calculated at the primitive level. Furthermore, we have extracted the EEG feature via autoregressive model, discrete wavelet transform, and fast Fourier transform. All eight features of the individual piece are combined to form a single feature distribution.

1) Autoregressive Model: Since an autoregressive (AR) model is known to limit the loss of spectral problems and to yield improved frequency resolution compared to nonparametric approach [1], we use AR to extract EEG features. AR model is achieved by calculating the coefficients of the linear system:

$$X_t = \sum_{i=1}^{p} a_i x_{t-i} + \varepsilon_t, \tag{1}$$

where X_t is the signal at the sampled point t, p is the order of the model, a_i is the AR coefficient, and ε_t is an independent and identically distributed white noise input [20]. In our system, the Yule-Walker method was used for AR spectral estimation [11]. Before employing the AR model, an optimal order was computed using the Levinson-Durbin method. This method fits an AR model to the auto-correlation sequence of interest and minimizes the model error.

2) Discrete Wavelet Transform: The wavelet transform is a spectral estimation method in which any function can be written as an infinite series of wavelets. It condenses the time varying signals with many data points into several small parameters that represent the signal [8]. Mathematically, the discrete wavelet transform (DWT) of a signal, $x(t)$, is the integral of the signal multiplied by scaled and shifted wavelet function ψ [29]. It is defined by:

$$DWT\,(j,k) = \frac{1}{\sqrt{|2^j|}} \int_{-\infty}^{\infty} x\,(t)\,\psi\left(\frac{t-2^j k}{2j}\right) dt, \tag{2}$$

where 2^j and $k2^j$ are called the scaling and time location or shifting parameters respectively [29].

The discrete wavelet transform is particularly suitable for analysis of sudden and transient signal changes. Since our signal is elicited by instantaneous visual stimuli, the discrete wavelet transform is suitable for our dataset [1].

3) Fast Fourier Transform: Fast Fourier transform (FFT) is widely used for many applications related to the EEG data analysis and signal processing in general. It quickly computes the discrete Fourier transform (DFT), which reduces the number of computations needed for N points from $2N^2$ to $2NlogN$, where log is the base-2 logarithm. Consider a complex series x(k) of length N where x is a complex number $x_i = x_{real} + x_{imag}$. Assume that the series outside the range 0, $N-1$ is extended N-periodic, where $x_k = x_{k+N}$ for all k [5]. Then, this transform is defined as follows:

$$x_k = \sum_{n=0}^{N-1} x_n \cdot e^{-i2\pi kn/N}. \tag{3}$$

The advantages of implementing the fast Fourier transform are the enhancement of speed over virtually all other available methods for real-time applications and improvement in the performance for the narrow-band signal like our EEG signals [1].

B. Mallows Distance

After combining the aforementioned features into a cluster with respect to time, we compute the distance between the current cluster and past EEG signal clusters using Mallows distance. Our distance measure has its root in measuring the difference between two multi-variable probability distributions. In 1972, Mallows proposed a Mallows distance to measure the difference between two probability distribution P and Q in R^d with the random variables X and Y [27]. It is defined by a minimum of the expected difference between X and Y overall joint probability distributions F for (X,Y) such that the marginal distribution of X is P and the marginal distribution of Y is Q [23]:

$$Mallows_p\,(P,Q) = min_F\left\{E_F\left\|X-Y\right\|^p\right\}^{1/p}, \tag{4}$$

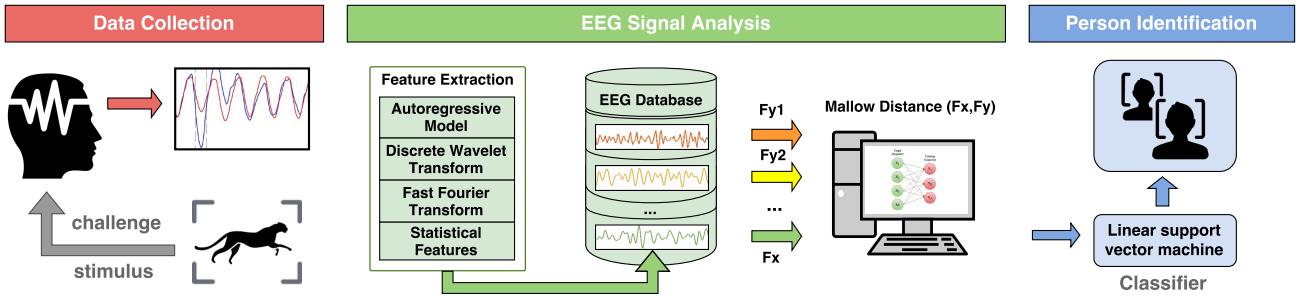

Fig. 3. EEG-based identification system framework.

TABLE I
FIVE STATISTICAL FEATURES AT THE PRIMITIVE LEVEL [38]

Statistical features	Definition
Mean	The average value of the signal over the window
Standard Deviation	Measure of dispersion of the signal over the window
Root Mean Square	The quadratic mean of the signal over the window
Average Derivatives	The average of the first order derivatives of the signal over the window
Level Crossing Rate	The total rate of signal crossing the mean level of the signal with a positive slope

subject to:

$$\int_Y dF(X,Y) = P(X), \int_X dF(X,Y) = Q(Y), \quad (5)$$

where p is some value greater or equal to 1. $\|.\|$ indicates the Euclidean length. In theory, Mallows distance can be computed both for discrete or continuous distribution [23]. Since we formulate the task of matching as a transportation problem between two solid feature set, our distributions are discrete. The discrete distributions $P = \{(x_1, p_1) \cdots (x_m, p_m)\}$, $1 \leq i \leq m$, and $Q = \{(y_1, q_1) \cdots (y_n, q_n)\}$, $1 \leq j \leq n$ with the weights add up to 1 ($\sum p_i = 1$ and $\sum q_j = 1$). Task is to minimize the expectation under the joint distribution $F = (f_{ij})$:

$$E_F \|X - Y\|^p = \sum_{i=1}^{m}\sum_{j=1}^{n} f_{ij} \|x_i - y_j\|^p = \sum_{i=1}^{m}\sum_{j=1}^{n} f_{ij} d_{ij}, \quad (6)$$

with subject to

$$f_{ij} \geq 0; 1 \leq i \leq m, 1 \leq j \leq n, \quad (7)$$

$$\sum_{j=1}^{n} f_{ij} = p_i; 1 \leq i \leq m, \quad (8)$$

$$\sum_{i=1}^{m} f_{ij} = q_j; 1 \leq j \leq n, \quad (9)$$

$$\sum_{i=1}^{m}\sum_{j=1}^{n} f_{ij} = \sum_{i=1}^{m} p_i = \sum_{j=1}^{n} q_j = 1. \quad (10)$$

In terms of the Earth Mover's Distance (EMD), a special case of the mass transport problem [35], constraint 1 shown in Eq. (7) allows the flow from P to Q but not from Q to P. Since both P and Q are probability distributions with a total mass of 1, weight normalization is not needed. Constraint 2 and 3 shown in Eq. (8) and 9 indicate that the number of supplies that can be sent by the clusters in P is equal to their weights, and the amount of cluster in Q is equal to their weight, respectively. Constraint 4 shown in Eq. (10) matches the clusters in two clusterings in a globally optimal manner. Therefore, it allows the tolerance in the EEG signal noises [23].

When Mallows distance is simplified with two samples of the same size $X = \{x_1, \cdots, x_n\}$ and $Y = \{y_1, \cdots, y_n\}$, the Mallows distance between empirical distribution is:

$$Mallows_p(X,Y) = \left(\frac{1}{n} min_{(j_1,\cdots,j_n)} \sum_{i=1}^{n} \|x_i - y_{j_i}\|^p\right)^{\frac{1}{p}}, \quad (11)$$

where the minimum is taken over every possible permutations of $\{1, \cdots, n\}$ [23]. It gives every point the weight of $\frac{1}{n}$.

C. Subject Identification

To generate the final decision of identification, we implement a linear support vector machine (SVM) to execute multi-class feature classification. Linear SVM is a particular linear discriminant classifier, which is known as one of the best classification methods with many computational advantages [15]. With the SVM, the points in space are divided into separate categories by a clear gap that is as wide as possible. Then, new sets are mapped to predict which category it belongs to based on which side of the gap they are located [7].

To strictly test the SVM model and prevent the model from being overfitted on existing data, we implement the k-fold cross-validation, with k being 10. The data set is randomly separated into 10 equal-sized subsets, for each trial, one of 10 subsets is used as a test set and other 9 subsets are used as a

training set. Each subset will be treated as a unique class in SVM to obtain the prediction result that enables true positive (TP), true negative (TN), false positive (FP), false negative analysis (FN). This cross-validation is repeated 10 times with each of 10 subsets used exactly once as the validation data. This process occurred separately from channel to channel. Overall, each cross-validation trial data will have 2 channels, and 10 subsets. The resulting model allows rapid subject prediction, per subject prediction duration is determined to be 0.1 seconds from 10 class prediction during each trial of 10-fold cross-validation.

IV. Performance Evaluation

To evaluate the effectiveness of Mallow distance on the EEG-based identification, we test our system performance using various performance metrics. The metrics include the average accuracy (ACC), balanced accuracy (BAC), f-score (f-1), receiver operating characteristics (ROC), and the half total error rate (HTER). Utilizing these metrics, we compare Mallows distance's performance against performance when utilizing DWT and Euclidean distance, the results are discussed in Sec. IV-C.

A. Evaluation Description

We first arrange the form of EEG signal in groups for systematic evaluation.

A single EEG signal is composed of brainwave responses on 10 visual stimuli. Since each participant experimented on 4 series of the task with 50 target stimuli each, there is a total of 20 EEG samples per person per channel (O1 and O2). Moreover, the performance of each channel is investigated, separately. Thus, with 10 subjects, there is a total of 200 EEG distributions for O1 and 200 EEG distributions for O2. Then, the dissimilarity computation is conducted on EEG distributions of O1 and O2, separately. In other words, one feature distribution from O1 of one subject is selected as a target data, and the rest distributions are considered as a training set. Then, the distance between each target and training pair is computed via Mallows distance. This process repeats for every other 199 distribution. Then, calculated distances undergo the SVM classification with 10-fold cross-validation. This procedure repeats for O2 EEG distributions.

Further, the performance of Mallows distance is compared with the performance of other distances, such as dynamic time warping (DTW) and Euclidean distance (ED). Definition of dynamic time warping for clustering EEG waveform is described in [18], and the definition for Euclidean distance on the signals is found in [17].

B. Evaluation Results

1) Accuracy: To measure the system performance, the average accuracy, balanced accuracy, and f-score accuracy are investigated. First accuracy metric, (ACC), is defined as:

$$Accuracy(\%) = \frac{TP + TN}{TP + FP + TN + FN} \tag{12}$$

where TP is a true positive, TN is a true negative, FP is a false positive, and FN is a false negative. Although the ACC assesses the accuracy of the system in a straight forward fashion, the number of negative classes 180, out-weights the number of positive classes 20. This unbalanced number classes can result in negative class heavy biase, which leads to imperfection. Thus, we implement additional metrics for classifier evaluation as follow.

Balanced accuracy metric (BAC) is adopted to handle the class imbalance. By definition, BAC is the arithmetic mean of sensitivity and specificity, and it is known for avoiding inflated performance estimates on the imbalanced dataset.

$$BAC(\%) = \frac{TP}{2(TP + FN)} + \frac{TN}{2(TN + FP)}. \tag{13}$$

Further, we calculate an f-score accuracy measure (f-1) to avoid the class imbalance. It is known as a harmonic mean of precision and recall because the recall and precision are evenly weighted. Mathematically, the f-score is defined as:

$$F_1(\%) = \frac{2TP}{2TP + FP + FN}. \tag{14}$$

The system performance on channel O1 and O2 are summarized in Table. II and Fig. 4. The average precision and recall of O1 are 95.90% and 95.50% with ACC of 99.10%, BAC of 97.50%, and f-score of 95.70%. The average precision and recall of O2 are 96.80% and 96.50% with ACC of 99.30%, BAC of 98.06%, and f-score of 96.65%. This implies that using O1 and O2, our system can correctly identify people with the average recall value of 96.00**%** and the average f-score of 96.18**%**. As expected, there was a slight discrepancy between ACC and the other two metrics in both O1 and O2 results. Despite the imbalance induced bias toward higher percentage accuracy in terms of ACC for both O1 and O2, the value alone shows a very similar relationship.

In addition, we draw the conclusion that overall TN percentage is higher than TP percentage based on the discrepancy.

The f-score of O2 is higher than that of O1 by 0.95%. However, our system still employs both O1 and O2 because their difference in the accuracy is negligible and several subjects perform better in O1. For instance, subject 6 performs better with O1 than O2 as he achieved higher accuracy for O1 (see Fig. 4(a)) than O2 (see Fig. 4(b)).

TABLE II
System performance

Distance Metrics	ACC (%)	BAC (%)	F1 (%)
O1	99.10	97.50	95.70
O2	99.30	98.06	96.65

2) Receiver operating characteristic: For a comprehensive analysis of the system performance, a receiver operating characteristic curve (ROC) is employed to evaluate our system (see Fig. 5(a) and Fig. 5(b)). By definition, ROC visualizes the sensitivity against FPR (false positive rate) as the threshold is varied. If the ROC curve follows the top-left corner of the graph, the system shows high sensitivity and specificity.

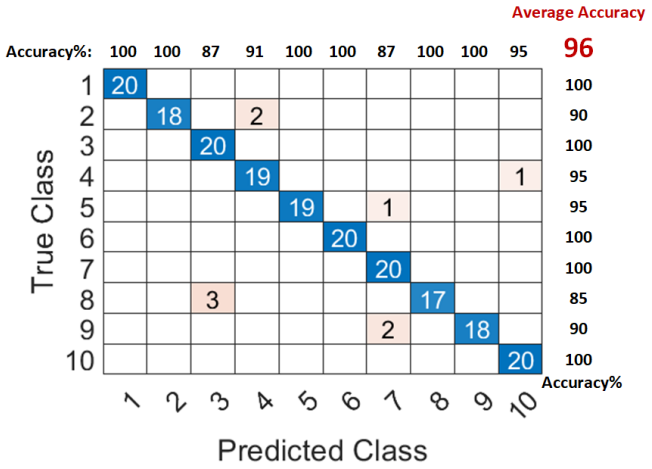

(a) Confusion matrix for O1.

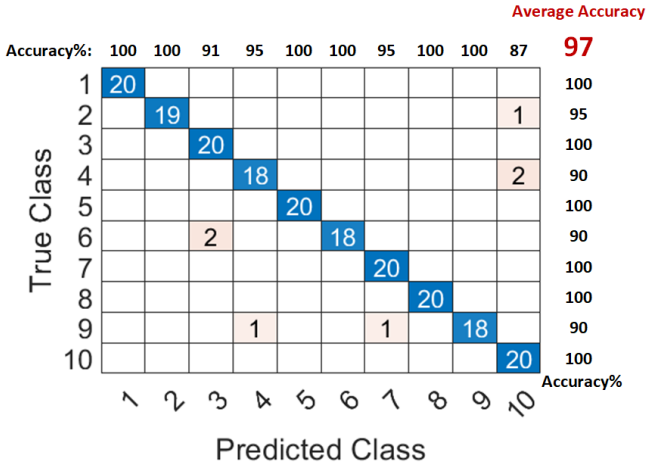

(b) Confusion matrix for O2.

Fig. 4. Confusion matrices for channel O1 and O2. Correctly classified subjects are colored in blue, and incorrectly classified subjects are colored in red. The depth of color signify the rate of occurrence. The rightmost column presents the recall (%), and the top row presents the precision (%) of each subject. The upper right corner shows the f-score (%).

Figure 5(a) and Figure 5(b) demonstrate the ROC curves for channel O1 and O2. Two figures illustrate that the performance of the majority of subjects is similar except for subject 8. The curve of subject 8 is slightly lower for O1, and this complies with the result shown in Fig. 4(a). Overall, most ROC curves follow the top-left corner of the graph, signifying that our system is robust and feasible.

3) Half total error rate: Half total error rate (HTER) is a way to measure the detection performance, which is popularly used as accuracy metrics for biometrics identification. HTER is defined in the following formula:

$$HTER = \frac{FAR + FRR}{2} \quad [\%], \tag{15}$$

where FAR refers to the false accept rate, and FRR indicates the false rejection rate.

Figure 6(a) illustrates the FRR, FAR, and HTER of 10 subjects on channel O1. The error bar represents the standard

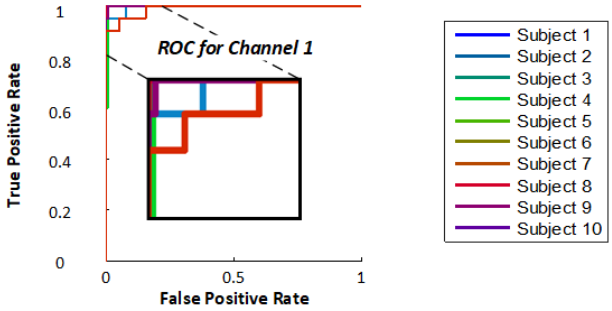

(a) The average ROC curves of 10 subjects on Channel O1.

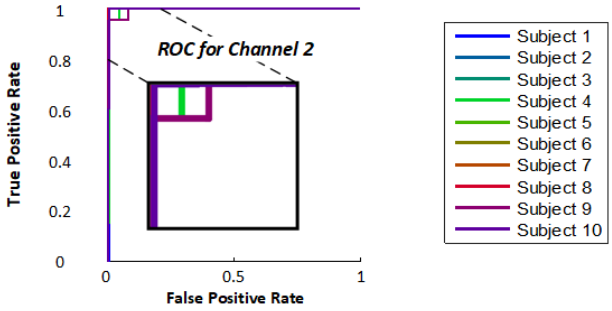

(b) The average ROC curves of 10 subjects on Channel O2.

Fig. 5. Receiver operating characteristic curves with 10 subjects. Close-up images are also shown.

deviation of each metric, and the red line in the box indicates the median value. The average FRR and FAR value for O1 are 4.500% and 0.501% with the standard deviation of 5.503% and 0.716%. When averaging two values, we achieved the HTER value of 2.501% with the standard deviation of 2.599%.

Figure 6(b) shows the FRR, FAR, and HTER for channel O2. The average FRR and FAR value for 10 subjects on O2 are 3.500% and 0.390% with the standard deviation of 4.743% and 0.590%, respectively. HTER value for O2 is 1.945% with its standard deviation of 2.295%. Therefore, the overall performance of our system using both O1 and O2 achieves the FRR of 4.000%, FAR of 0.446%, and HTER of 2.223%. For both O1 and O2, FAR is much lower than FRR because our negative class outnumbers the positive class.

Compared to the performance of O2, O1 provides higher FRR, FAR, and HTER by 1.000%, 0.740%, and 0.556%. This result indicates that the signals acquired from O1 are less likely to identify individuals accurately compared to O2. However, as addressed above, both channels are used for the system because the performance of an individual varies from channel to channel.

C. Comparison with other distance metrics

To illustrate the performance improvement of classification utilizing Mallows distance, we exhibit the classification performance of different distance metrics.

Table III shows a summary of the performance measures of Mallows distance, dynamic time warping (DTW), and

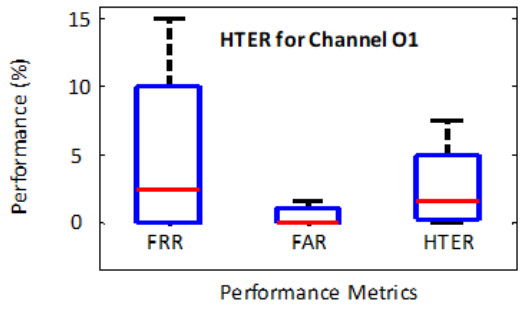

(a) Boxplot of FRR, FAR, and HTER for channel O1.

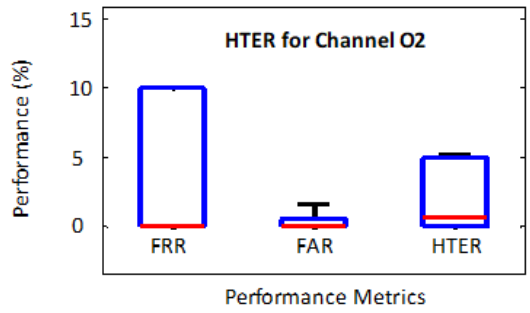

(b) Boxplot of FRR, FAR, and HTER for channel O2.

Fig. 6. Boxplot for channel O1 and O2. The red line indicates the median value among 10 subjects. The standard deviation is represented by the error bars in black color.

Euclidean distance. The testing performance of Mallows distance is found to be satisfactory compared to that of DTW and Euclidean distance. Specifically, the f-score of Mallows distance is higher than that of DTW and Euclidean distance by 2.31% and 6.48%, respectively. This proves that there is a significant performance advantage for adopting Mallows distance over DTW and Euclidean distance.

TABLE III
PERFORMANCE COMPARISON

Distance Metrics	ACC (%)	BAC (%)	F1 (%)
Mallows	99.20	97.78	96.18
DTW	97.60	94.23	93.87
Euclidean	94.82	90.88	89.70

While Euclidean distance has an advantage of simple and fast calculation, it is unreliable when one of the features has a relatively large quantity and overpowers the other. The inevitable imbalance of feature weight weakens the accuracy of using Euclidean distance. Due to this weakness, Euclidean distance demonstrates the lowest performance as shown in Table. III. On the other hand, DTW allows two-time series that are similar but locally out of phase to align in a non-linear manner, thereby resolves the problem of Euclidean distance [33]. Still, DTW algorithm is inevitable from one critical problem; it may not detect obvious alignments in two signal if a feature of one signal is slightly higher or lower than its corresponding feature of the other signal [4], [22]. Therefore, DTW is vulnerable to noises and provides less accuracy than Mallows distance. Mallows distance, which uses a clustering comparison, is robust to the signal noises and shows a better performance than two metrics in a statistical manner. Thus, Mallows distance is suitable for EEG-based subject identification.

D. Impact of stimuli types

In this section, we investigate the performance of the EEG responses generated by non-target stimuli with 10 participants. Table IV summarizes the average performance (O1 and O2) with FRR, FAR, and HTER for target and non-target stimuli. When the target stimuli are employed, the average FRR and FAR value are 4.000% and 0.446% with the standard deviation of 5.026% and 0.641%, respectively. Therefore, the EEG signals that are generated by target stimuli provide the HTER of 2.223% with the standard deviation of 2.4029%. When EEG signals are evoked by non-target stimuli, our system achieves the FRR of 6.250%, FAR of 0.695% and HTER of 3.473% with the standard deviation of 7.927%, 0.968% and 4.125%, correspondingly. For both target and non-target, the horizontal line in the box plots for FRR and FAR is absent because their median value for FRR and FAR is 0. Performance comparison between target and non-target stimuli are illustrated in Fig. 7. In general, FRR, FAR and HTER of the target stimulation are lower than FRR, FAR and HTER of the non-target stimulation by 2.250%, 0.249%, and 1.250%. Thus, the stimulation of target images provides better performance than the presentation of non-target images. This result suggests that the target stimuli generate more distinguishable EEG responses than the non-target stimuli during the categorization task.

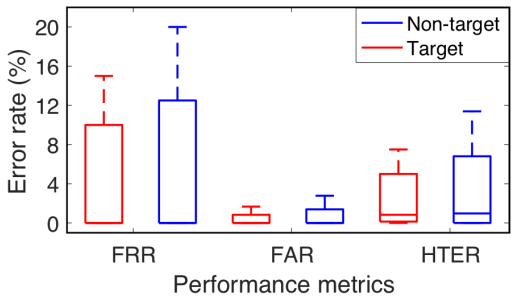

Fig. 7. Boxplot of FRR, FAR, and HTER with target and non-target stimuli. The horizontal line in the box indicates the median value, and error bar represents the standard deviation.

V. CONCLUSION

In this paper, we addressed the EEG-based personal identification method using Mallows distance. Unlike previously published works, we utilize Mallows distance calculation for EEG signal cluster model for personal identification process.

TABLE IV
ERROR RATES FOR TARGET AND NON-TARGET STIMULUS

Type	FRR (%)	FAR (%)	HTER (%)
Target	4.000	0.446	2.223
Non-target	6.250	0.695	3.473

We first investigate and apply Mallow distance to EEG signal from healthy participants in existing database. Statistical features, autoregressive model, discrete wavelet transform, and fast Fourier transform have been utilized for feature extraction methods. We then implement SVM to classify EEG features for independent participant to validate the concept of using Mallows distance to perform EEG biometric identification. After classification, we perform extensive analysis on performance which yielded the classification score of 96.18%. This result reveals the high feasibility of using Mallows distance based EEG feature to serve as biometric identification.

ACKNOWLEDGEMENT

This work is in part supported by the US National Science Foundation under grant No. 1564104/1840790.

REFERENCES

[1] A. S. Al-Fahoum and A. A. Al-Fraihat. Methods of eeg signal features extraction using linear analysis in frequency and time-frequency domains. *ISRN neuroscience*, 2014, 2014.

[2] S. Altahat, M. Wagner, and E. M. Marroquin. Robust electroencephalogram channel set for person authentication. In *2015 IEEE International Conference on Acoustics, Speech and Signal Processing (ICASSP)*, pages 997–1001. IEEE, 2015.

[3] B. W. Beenau, D. S. Bonalle, S. W. Fields, W. J. Gray, C. Larkin, J. L. Montgomery, and P. D. Saunders. Method and system for dna recognition biometrics on a fob, Oct. 17 2006. US Patent 7,121,471.

[4] B. Ben Ali, Y. Masmoudi, and S. Dhouib. Accurate and fast dynamic time warping approximation using upper bounds. In *Telecommunications and Signal Processing (TSP), 2015 38th International Conference on*, pages 1–6. IEEE, 2015.

[5] P. Bourke. Dft (discrete fourier transform) fft (fast fourier transform). *Internet, http://astronomy. swin. edu. au/˜ pbourke/analysis/dft*, 1993.

[6] C. B. Brumback, N. A. Myers, S. G. J. Yuen, J. Park, and T. S. Diemer. Biometric monitoring device with heart rate measurement activated by a single user-gesture, May 26 2015. US Patent 9,042,971.

[7] C. Cortes and V. Vapnik. Support-vector networks. *Machine learning*, 20(3):273–297, 1995.

[8] D. Cvetkovic, E. D. Übeyli, and I. Cosic. Wavelet transform feature extraction from human ppg, ecg, and eeg signal responses to elf pemf exposures: A pilot study. *Digital signal processing*, 18(5):861–874, 2008.

[9] A. Delorme, G. A. Rousselet, M. J.-M. Macé, and M. Fabre-Thorpe. Interaction of top-down and bottom-up processing in the fast visual analysis of natural scenes. *Cognitive Brain Research*, 19(2):103–113, 2004.

[10] S. C. for Computational Neuroscience Foundation (SCCN). Eeg/erp data available for free public download, Dec. 2013. Last accessed 10 April 2016.

[11] B. Friedlander and B. Porat. The modified yule-walker method of arma spectral estimation. *IEEE Transactions on Aerospace and Electronic Systems*, (2):158–173, 1984.

[12] Q. Gui, Z. Jin, M. R. Blondet, S. Laszlo, and W. Xu. "towards eeg biometrics: Pattern matching approaches for user authentication". In *IEEE International Conference on Identity, Security and Behavior Analysis (ISBA'15)*, pages 1 – 7, Kong Hong, March 2015.

[13] Q. Gui, Z. Jin, and W. Xu. Exploring EEG-based Biometrics for User Identification and Authentication. In *the IEEE Signal Processing in Medicine and Biology Symposium (SPMB'14)*, pages 1 – 6, Philadelphia, Pennsylvania, USA, December 2014.

[14] Q. Gui, Z. Jin, W. Xu, M. V. Ruiz-Blondet, and S. Laszlo. Multichannel eeg-based biometric using improved rbf neural networks. In *2015 IEEE Signal Processing in Medicine and Biology Symposium (SPMB)*, pages 1–6, Dec 2015.

[15] I. Guyon, J. Weston, S. Barnhill, and V. Vapnik. Gene selection for cancer classification using support vector machines. *Machine learning*, 46(1-3):389–422, 2002.

[16] N. Hazarika, J. Z. Chen, A. C. Tsoi, and A. Sergejew. Classification of eeg signals using the wavelet transform. In *Digital Signal Processing Proceedings, 1997. DSP 97., 1997 13th International Conference on*, volume 1, pages 89–92. IEEE, 1997.

[17] M. Helen and T. Virtanen. Query by example of audio signals using euclidean distance between gaussian mixture models. In *Acoustics, Speech and Signal Processing, 2007. ICASSP 2007. IEEE International Conference on*, volume 1, pages I–225. IEEE, 2007.

[18] H.-C. Huang and B. Jansen. Eeg waveform analysis by means of dynamic time-warping. *International journal of bio-medical computing*, 17(2):135–144, 1985.

[19] A. K. Jain, K. Nandakumar, and A. Nagar. Biometric template security. *EURASIP Journal on advances in signal processing*, 2008:113, 2008.

[20] S. Jain and G. Deshpande. Parametric modeling of brain signals. In *Biotechnology and Bioinformatics, 2004. Proceedings. Technology for Life: North Carolina Symposium on*, pages 85–91. IEEE, 2004.

[21] N. Juel-Nielsen and B. Harvald. The electroencephalogram in uniovular twins brought up apart. *Human Heredity*, 8(1):57–64, 1958.

[22] E. J. Keogh and M. J. Pazzani. Derivative dynamic time warping. In *Sdm*, volume 1, pages 5–7. SIAM, 2001.

[23] E. Levina and P. Bickel. The earth mover's distance is the mallows distance: some insights from statistics. In *Computer Vision, 2001. ICCV 2001. Proceedings. Eighth IEEE International Conference on*, volume 2, pages 251–256. IEEE, 2001.

[24] Z. Li, Y. Wang, A. S. Rathore, C. Song, N. Nyayapathi, T. Vu, J. Xia, and W. Xu. Pavessel: Practical 3d vessel structure sensing through photoacoustic effects with its applications in palm biometrics. *Proc. ACM Interact. Mob. Wearable Ubiquitous Technol.*, 2(3):122:1–122:24, Sept. 2018.

[25] F. Lin, K. W. Cho, C. Song, W. Xu, and Z. Jin. Brain password: A secure and truly cancelable brain biometrics for smart headwear. In *Proceedings of the 16th Annual International Conference on Mobile Systems, Applications, and Services*, MobiSys '18, pages 296–309, New York, NY, USA, 2018. ACM.

[26] F. Lin, C. Song, Y. Zhuang, W. Xu, C. Li, and K. Ren. Cardiac scan: A non-contact and continuous heart-based user authentication system. In *Proceedings of the 23rd Annual International Conference on Mobile Computing and Networking*, MobiCom '17, pages 315–328, New York, NY, USA, 2017. ACM.

[27] C. L. Mallows. A note on asymptotic joint normality. *The Annals of Mathematical Statistics*, 43(2):508–515, 1972.

[28] G. Mohammadi, P. Shoushtari, B. Molaee Ardekani, and M. B. Shamsollahi. Person identification by using ar model for eeg signals. In *Proceeding of World Academy of Science, Engineering and Technology*, volume 11, pages 281–285, 2006.

[29] H. Ocak. Automatic detection of epileptic seizures in eeg using discrete wavelet transform and approximate entropy. *Expert Systems with Applications*, 36(2):2027–2036, 2009.

[30] O. R. Patil, W. Wang, Y. Gao, W. Xu, and Z. Jin. A non-contact ppg biometric system based on deep neural network. In *2018 IEEE 9th International Conference on Biometrics Theory, Applications and Systems (BTAS)*, pages 1–7, Oct 2018.

[31] M. Poulos, M. Rangoussi, N. Alexandris, A. Evangelou, et al. Person identification from the eeg using nonlinear signal classification. *Methods of information in Medicine*, 41(1):64–75, 2002.

[32] K. B. Raja, R. Raghavendra, V. K. Vemuri, and C. Busch. Smartphone based visible iris recognition using deep sparse filtering. *Pattern Recognition Letters*, 57:33–42, 2015.

[33] C. A. Ratanamahatana and E. Keogh. Everything you know about dynamic time warping is wrong. In *Third Workshop on Mining Temporal and Sequential Data*. Citeseer, 2004.

[34] G. Repovs. Dealing with noise in eeg recording and data analysis. In *Informatica Medica Slovenica*, volume 15, pages 18–25, 2010.

[35] Y. Rubner, C. Tomasi, and L. J. Guibas. The earth mover's distance as a metric for image retrieval. *International journal of computer vision*, 40(2):99–121, 2000.

[36] A. Subasi. Eeg signal classification using wavelet feature extraction and a mixture of expert model. *Expert Systems with Applications*, 32(4):1084–1093, 2007.

[37] Y. Tian, Y. Li, X. Liu, R. H. Deng, and B. Sengupta. Pribioauth: Privacy-preserving biometric-based remote user authentication. In *2018 IEEE Conference on Dependable and Secure Computing (DSC)*, pages 1–8. IEEE, 2018.

[38] M. Zhang and A. A. Sawchuk. Motion primitive-based human activity recognition using a bag-of-features approach. In *Proceedings of the 2Nd ACM SIGHIT International Health Informatics Symposium*, IHI '12, pages 631–640, New York, NY, USA, 2012. ACM.

[39] D. Zhou, J. Li, and H. Zha. A new mallows distance based metric for comparing clusterings. In *Proceedings of the 22nd international conference on Machine learning*, pages 1028–1035. ACM, 2005.